

https://dspace.org/

Analysis of the Hadley cell subtropical anticyclones and their effects on South African rainfall

Dawn Mahlobo; Francois Engelbrecht; Thando Ndarana; Hadisu Abubakar; Mary Funke Olabanji ...

https://hdl.handle.net/10539/41078
WOS

Downloaded from a DSpace repository. https://dspace.org/

Theoretical and Applied Climatology (2024) 155:1035–1054
https://doi.org/10.1007/s00704-023-04674-z

RESEARCH

Analysis of the Hadley cell, subtropical anticyclones and their effect on South African rainfall

Dawn Mahlobo[1,2] · Francois Engelbrecht[2] · Thando Ndarana[3] · Hadisu Bello Abubakar[2,4] · Mary Funke Olabanji[5] · Katlego Ncongwane[1]

Received: 6 July 2022 / Accepted: 22 September 2023 / Published online: 11 October 2023
© The Author(s) 2023

Abstract
This study investigates the behaviour of subtropical high-pressure systems and the Hadley cell, which affect the weather of South Africa, using the ERA-Interim database and ensemble of 14 global circulation models from Phase 6 of the Coupled Model Intercomparison Project (CMIP6). Mass stream function was used to represent the Hadley cell. To analyse the behaviour of the subtropical anticyclones, monthly sea level pressure, the 1018 hPa isobar and the maximum isobar in the study area were used. The seasonal variation of the anticyclones and Hadley circulation is consistent with rainfall over South Africa. During austral summer, a less intense, narrow mass stream function, South Atlantic Subtropical Anticyclone and Mascarene High are located more southwards, causing rainfall over the eastern parts of South Africa. During the austral winter, Hadley circulation, as well as the anticyclones, is stronger and located more northwards, causing rainfall over the southern and southwestern parts of South Africa.

1 Introduction

The Hadley cell (HC), defined as the zonally averaged meridional overturning motion that links the tropics and mid-latitudes, plays an essential role in global atmospheric general circulation by transporting momentum polewards (Holton and Hakim 2012). Changes in the HC have been examined using observational datasets, reanalysis techniques and model simulations (Lu et al. 2007; Frierson et al. 2007; Hu et al. 2013). Through the utilisation of global circulation models derived from the Coupled Model Intercomparison Project (CMIP)'s Phase 3 experiment, it has been established that the expansion of the HC can be linked to the escalating concentration of greenhouse gases (GHGs) (Lu et al. 2007; Frierson et al. 2007). Hu et al. (2013) used CMIP5 simulations to demonstrate the widening of the HC. Through the analysis of satellite-borne microwave sounding unit data, Fu et al. (2006) demonstrated the expansion of the HC, whereas Seidel and Randel (2007), utilising radiosonde data, highlighted the intensification of the HC. Examining the changes in the HC over centennial time scales (1871–2008), Liu et al. (2012) utilised reanalysis data and found evidence of intensification at those extended scales. The HC was found to be intensifying. Several studies documented large seasonal variations of the HC widening and intensifying using reanalysis data (e.g. Nguyen et al. 2013, 2015; Schwendike et al. 2014, 2015; Mahlobo et al. 2018; Diaz and Bradley 2004; Mitas and Clement 2005). The widening of the HC by 2−5° has been shown using observed outgoing longwave radiation (OLR) and model simulations (Johanson and Fu 2009). The HC plays an integral role in anthropogenic-induced climate

✉ Dawn Mahlobo
ddmahlobo@gmail.com

Francois Engelbrecht
Francois.Engelbrecht@wits.ac.za

Thando Ndarana
Thando.ndarana@up.ac.za

Hadisu Bello Abubakar
guidenet80@gmail.com

Mary Funke Olabanji
Real.funky@yahoo.com

Katlego Ncongwane
Katlego.ncongwane@weathersa.co.za

1 South African Weather Service, Pretoria, South Africa

2 Present Address: Global Change Institute, Wits University, Johannesburg, South Africa

3 Department of Geography, Geoinformatics and Meteorology, University of Pretoria, Pretoria, South Africa

4 School of Animals, Plants and Environment, Wits University, Johannesburg, South Africa

5 National Biotechnology Development Agency, Abuja, Nigeria

change and associated changes in atmospheric circulation. Several studies allude for progressive HC expansion (e.g. Hu et al. 2013; Johanson and Fu 2009; Mahlobo et al. 2018; Nguyen et al. 2013), increased frequency of higher subtropical tropopause heights and the widening of the subtropical dry zones. (Seidel and Randel 2007). The expansion of the HC is solely due to an increase in GHG concentrations in the atmosphere (Lu et al. 2007). GHG concentrations are projected to further increase in the future under various mitigation scenarios (Solomon et al. 2007). The HC will hence continue to expand under the low mitigation scenario (RCP8.5) (Johanson and Fu 2009).

The poleward edge of the HC has been displaced poleward during the twenty-first century, expanding the subtropical belts and intensifying aridity (Yin 2005). The subtropical belts feature cool and surface-divergent air that sinks from the upper levels, where air converges from the tropical and temperate belts (Tyson and Preston-Whyte 2000). Subtropical anticyclones and low-level synoptic-scale weather systems play a pivotal role in the climate system over the subtropics (Cherchi et al. 2018). Li et al. (2012) found substantial subsidence, predominantly on the eastern sides of these subtropical anticyclones. The semi-permanent subtropical anticyclones persist for most of the year in specific locations (Ynoue et al. 2017). Semi-permanent anticyclones are characterised by mean anticyclone flow, subsidence and lower-level divergence (Reboita et al. 2019), resulting from the descending HC limb (Tyson and Preston-Whyte 2000). In fact, the climate of the earth's arid and semiarid regions is influenced by both the descending branch of the HC and the subtropical ridge (STR).

South Africa, in particular, is positioned in the descending branch of the HC, between the latitudes 22°S and 33°S. It is significantly influenced by the subtropical belt. Subtropical anticyclones dominate the South African interior in winter, intensifying at the end of austral winter and early spring (Seager et al. 2003; Lee et al. 2013), owing to the intensification of the HC (Mahlobo et al. 2018). Notably, three key subtropical anticyclones affect South Africa: the South Atlantic Subtropical Anticyclone (SASA) west of South Africa, the Kalahari Subtropical Anticyclone inland of South Africa and the Mascarene High east of South Africa (Xulu et al. 2020). The strengthening of the Kalahari anticyclone curtails frontal rainfall east and north of the Karoo and the Namib Deserts (Reason et al. 2002).

Subtropical anticyclones are associated with subsidence in the polar branch of the HC (Namias 1972; Rodwell and Hoskins 2001; Dima and Wallace 2003; Seager et al. 2003). Over the Southern Hemisphere, the SASA is more intense during austral winter (Seager et al. 2003; Lee et al. 2013) when surface atmospheric pressure is maximised due to the greater intensity of the HC (Rodwell and Hoskins 2001; Seager et al. 2003). Conversely, during spring-summer, subtropical anticyclones are better configured (Seager et al. 2003). Seager et al. (2003) further suggest that the seasonal cycle of subtropical anticyclones is associated with the seasonal variation of the sea surface temperature (SST). On average, the subtropical anticyclones move from their usual position eastward from day to day due to the positions, intensities and speeds of middle-latitude cyclones. They are normally stationary at 30°S, 10°W in the South Atlantic Ocean in summer. A ridge is formed as the anticyclones extend eastwards, or closed anticyclones sometimes drift past the land (Taljaard 1996). The system normally develops into a closed high-pressure cell in the western Indian Ocean. The ridge will sometimes extend northwards to the provinces of Limpopo and Mpumalanga (Taljaard 1996).

Changes in the HC have devastating consequences for weather and climate patterns, as evidenced in the occurrence of severe floods and droughts around the world (Allen et al. 2012; Chen and Held 2007; Freitas and Ambrizzi 2015). Connections between the HC and rainfall have been established in a number of studies (Kanamitsu and Krishnamurti 1978; Nicholson 1981; Hou and Lindzen 1992; Hoskins 1996; Yin 2005). Some of the earliest work found a positive correlation between the intensification and equatorward displacement of the northern Hadley circulation, and dry conditions over the northern tropical regions (Kanamitsu and Krishnamurti 1978). Nicholson (1981) suggested that changes in the HC have a major impact on rainfall fluctuations over West Africa. Over the eastern parts of southern Africa; the HC is normally associated with very wet summer months (Manabe and Holloway 1975), with particularly high rainfall over the eastern coasts during summer (Tyson and Preston-Whyte 2000). However, this association is stronger in winter when there are no other rainfall-producing systems (Hou and Lindzen 1992).

Alterations in the HC have reshaped the seasonal rainfall pattern across South Africa (Tyson and Preston-Whyte 2000). The country primarily experiences rainfall during the summer months (Roffe et al. 2019), with a pronounced zonal precipitation gradient between its eastern and western regions. During summer, the eastern side receives more rainfall (Roffe et al. 2019), while the western and southwestern coasts encounter reduced rainfall in winter. The winter rainfall zone mainly depends on frontal rain for its annual precipitation (Mahlalela et al. 2019). Pascale et al. (2020) found that the 2015−2017 winter season's rainfall deficit in South Africa coincided with positive anomalies in sea level pressure on the southern flank of the South Atlantic and South Indian subtropical highs.

Alongside the expansion of the HC, the intensity of Southern Hemisphere subtropical anticyclones is anticipated to increase, driven by elevated sea surface temperatures (Fahad et al. 2021). The poleward expansion of the HC in the changing climate suggests a drying trend at the latitude of Cape Town due to the associated southward shift

in the storm tracks (Burls et al. 2019). Moreover, the HC's descending limb is projected to intensify in the future, leading to reduced rainfall over southern Africa under low mitigation scenarios (Engelbrecht et al. 2009, 2011).

While the expansion of the HC trend and its implications for the South African climate have been established, the relationship between this expansion and South Africa's rainfall systems remains largely unexplored. Existing research has predominantly examined the Hadley cell, subtropical cyclones and South African rainfall discretely. This study, therefore, aims to collectively investigate the connection between the HC, the subtropical pressure systems and South African rainfall. Furthermore, it seeks to assess how the identified changes align with the representations in the CMIP6 models.

2 Data and methods

2.1 Data

The study investigates associations between the HC, subtropical anticyclones and their effect on South Africa's rainfall. Data used spans 1980 to 2018. Historical simulations of 14 global circulation models (GCMs) (Table 1) from the archive of Phase 6 of the Coupled Model Intercomparison Project (CMIP6) (Boer et al. 2016) and the European Centre for Medium-Range Weather Forecasts (ECMWF)'s Interim Reanalysis (ERA-Interim) database (Dee et al. 2011) were used in the study. The selection of the CMIP6 GCMs was based on the complete record of the meridional velocity, mean sea level pressure and rainfall data for the study period. The CMIP6 data is on a Gaussian grid and has different horizontal resolutions, as shown in Table 1. Therefore, to enable comparison between the GCMs and the ERA-Interim database, data was interpolated bicubically to a $0.75° \times 0.75°$ grid, which is the horizontal resolution of the ERA-Interim database. Meridional velocity from 1000 to 10 hPa was used to calculate the meridional mass stream function (MMS). The annual, seasonal and monthly means of the MMS are used to represent the HC. For the period of this study, the ERA-Interim reanalysis data was the latest global atmospheric reanalysis generated by the ECMWF. It thus integrates many important model improvements, such as resolution and physics changes, the use of four-dimensional variational data assimilation and various other changes in the analysis methodology (Trenberth et al. 2009). For the study period used, the ERA-Interim database was found to exceed other forms of reanalysis in terms of its performance (Lin et al. 2014; Jakobson et al. 2012).

2.2 Method

The study used the MMS to study the present-day simulations of the HC. The MMS is determined by vertically integrating the pressure-weighted, zonally averaged meridional wind v (Polvani et al. 2011):

$$\psi = \frac{2\pi a \cos\phi}{g} \int_{p}^{p_s} \bar{v} dp', \tag{1}$$

Table 1 CMIP6 global climate models used in this study

Modelling centre	Institute	Model name	Resolution (degrees east)
Atmosphere and Ocean Research Institute (University of Tokyo), National Institute for Environmental Studies and Japan Agency for Marine-Earth Science and Technology	MIROC	MIROC6	1.40625
Institute of Numerical Mathematics	INM	INM-CM4-8	2
Chinese Academy of Sciences	CAS	FGOALS-f3	1.25
Centre National de Recherches Météorologiques – Centre Européen de Recherche et de Formation Avancée en Calcul Scientifique	CNRM-CERFACS	CNRM-CM6	1.40625
European Community Earth Consortium	EC Earth Consortium	EC-Earth3	0.703125
Beijing Climate Center	BCC	BCC-CSM2-MR	1.125
Chinese Academy of Meteorological Sciences	CAMS	CAMS-CSM1-0	1.125
Institute Pierre-Simon, Laplace	IPSL	IPSL-CM6A-LR	2.5
National Institute of Meteorological Sciences/Korea Meteorological Administration (NIMS-KMA)	KACE	KACE-1-0-G	1.875
National Oceanic and Atmospheric Administration, Geophysical Fluid Dynamics Laboratory (NOAA-GFDL)	GFDL	GFDL-ESM4	1.25
National Center for Atmospheric Research (NCAR)	CESM2	CESM2-WACCM	1.25
Korea Institute of Ocean Science and Technology (KIOST)	KIOS	KIOST-ESM	1.875
Research Center for Environmental Changes (AS-RCEC)	TAI	TaiESM1	1.25

where ϕ represents latitude, a is the radius of earth, and other symbols have the conventional meaning. A clockwise circulation (such as the Northern Hemispheric HC) is defined as negative, while counter-clockwise circulations are positive.

The position and the strength of the subtropical anticyclones were determined by using the nearest-neighbour technique, which compares grid points within a specific domain to find the highest pressure, following Reboita et al. (2019). This method was applied over an area bounded by 10°E to 50°E and 0°S to 50°S. According to Reboita et al. (2019), the behaviour of the subtropical anticyclone can be analysed by considering a specific isobar line. In this study, the 1018 isobar line was used to analyse the climatology of the subtropical anticyclones affecting the weather of South Africa.

Linear trends were constructed of monthly, seasonal and annual MMS, mean sea level pressure and rainfall from the CIMP6 GCMs and the ERA-Interim database. Using the Student's t test, the 95% level of statistical significance of the trends was tested. CMIP6 GCMs were used to investigate future projections of the seasonal MMS, mean sea level for the high and low mitigation scenarios.

3 Results

3.1 Climatology

3.1.1 Annual climatology

The climatology of the subtropical higher-pressure cells that affect the weather and climate of South Africa is shown in Fig. 1A from the CMIP6 dataset and in Fig. 1D from the ERA-Interim dataset. The green shades depict areas of higher pressure, and the brown shades indicate areas of low pressure. Three semi-permanent high-pressure cells are evident from both datasets around latitudes 15°S to 39°S. Both datasets show the SASA west of the subcontinent, the Mascarene High in the east and the Kalahari High over the interior of the subcontinent. The three anticyclones are responsible for the climate of South Africa being characterised by low amounts of rainfall in the west. Towards the northern parts of the subcontinent, areas of low pressure are evident. The SASA is located west of South Africa and influences the weather of the western half of South Africa. Over the interior, the Kalahari His evident, which affects much of the weather over the interior, especially over the northwestern parts, while the eastern coastal areas are mostly affected by the Mascarene High. The Mascarene High may also cause atmospheric blocking, resulting in floods due to the landing of tropical cyclones (Xulu et al. 2020).

The annual rainfall climatology from both the ERA-Interim and CMIP6 ensemble mean data (Fig. 1C and F) show moderate amounts of rainfall over the interior of South Africa, with evidence of wetter conditions over the eastern parts and drier conditions over the western parts. Maximum amounts of rainfall are shown over the northwestern parts of the subcontinent. The CMIP6 ensemble mean of different GCMs' annual MMS (Fig. 1B) and the corresponding climatology from the ERA-Interim dataset (Fig. 1E) are also shown. The annual mean MMS from both datasets is characterised by an equatorially symmetric component, with ascent in the tropics and subsidence in the subtropics. According to Dima and Wallace (2003), the axis of symmetry is not exactly on the equator, but is located a few degrees away from the equator. The two symmetrical cells represent clockwise (blue shades) and anticlockwise (red shades) motions positioned in the Northern and Southern Hemispheres. The region of ascent in between the two cells is linked to the band of heavy near-equatorial rainfall, while dry zones are found at the descending limbs of the cells. The CMIP6 shows areas of higher MMS values for the clockwise circulation, while this feature is not evident in the ERA-Interim datasets. One notable feature of the anticlockwise circulation is that it is broader at the lower levels and becomes narrower at the upper levels. This feature has been captured well by the reanalysis, as well as in the CMIP6 models.

3.1.2 Seasonal climatology

Figure 2 shows the seasonal average of the mean sea-level pressure (MSLP) for the period 1979−2020 from the CMIP6 ensemble average and ERA-Interim database, respectively. Areas of higher pressure are depicted in shades of green, while the brown shades indicate areas of low pressure. During DJF and MAM (Fig. 2A, B, E and F) in both datasets, the SASA and Mascarene High are still evident, but are weaker and located more southwards. The Mascarene High brings onshore winds, transporting moist air from the ocean (Rapolaki et al. 2020), which will result in rainy conditions over the eastern parts of South Africa during the austral summer. Over the interior of the subcontinent, the Kalahari High lifts due to continental heating and moves southwards. A surface trough dominates the interior of South Africa. This brings in moist air over the interior, instigating cloud formation and rainfall. This is depicted by both the CMIP6 and ERA-Interim seasonal rainfall climatology, where rainfall is evident over the interior of South Africa (Fig. 3A and E). The rainfall decreases westwards, and no rainfall is observed over the western parts of South Africa. The ridging of the SASA from the south onto the land is also evident during DJF and MAM (Fig. 3A, B, E and F). As a matter of fact, when the Kalahari High or SASA are anomalously strong or located further south, the jet stream and South Atlantic storm tracks migrate southwards, resulting in weak and southwards-displaced frontal systems, and hence low

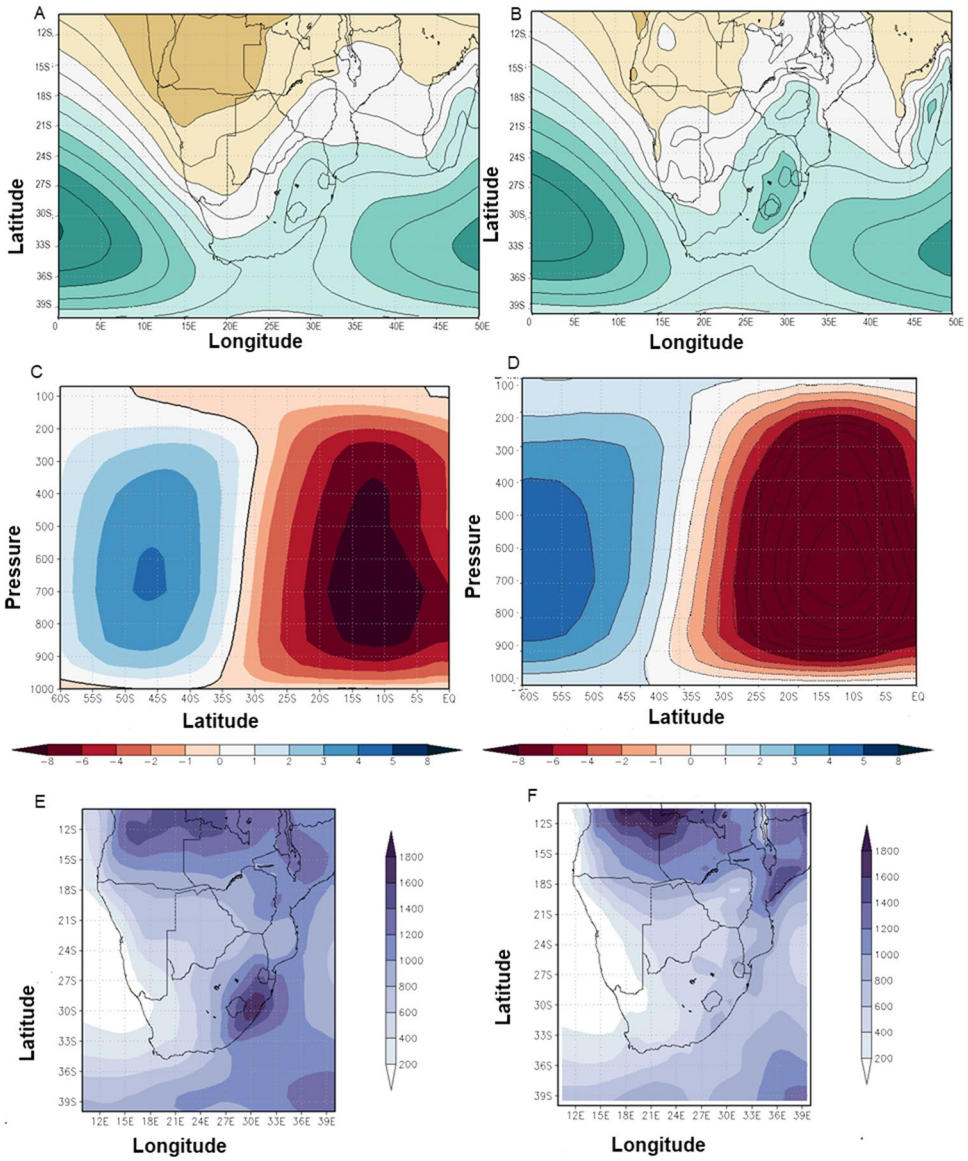


Fig. 1 Annual climatology of sea level pressure (hPa), mass stream function ($\times 10^9$ kg s^{-1}) and rainfall (mm) from the CMIP6 ensemble mean (**A**, **C** and **E**) and from the ERA-Interim (**B**, **D** and **F**) datasets, respectively. Green shades represent high-pressure values, and brown shades represent low-pressure values. Red shades represent anticlockwise circulation and blue shades represent clockwise circulation. Purple shades indicate rainfall amounts

winter rainfall over Cape Town (Sousa et al. 2018; Mahlalela et al. 2019). When comparing the two datasets, ERA-Interim shows strong (weak) anticyclones (low-pressure systems), while the CMIP6 ensemble shows stronger (weaker) low (high)-pressure systems.

The subtropical anticyclones are located more northwards during the austral winter (Fig. 2C and F). During the austral winter, the SASA ridges behind the mid-latitude cyclone south of the country to cause rainfall over the southern and southwestern parts of South Africa (Fig. 3C, D, G and H). The SASA brings in cold dry air to the western parts of South Africa. The Kalahari anticyclone dominates the interior of South Africa and is located more northwards. The landmass over the interior is colder, causing temperature inversion below the level of the escarpment. This inhibits moist air to reach the plateau. The descending air of the HC leads to stable conditions, clear skies and no rain over the plateau in winter. Hence, subsidence prevails over the country. The northward migration of the subtropical high leads to low-pressure anomalies and cyclonic circulation south of South Africa (Cook 2003; Vigaud et al. 2009), as well as high-pressure anomalies over the continent. This inhibits mid-latitude wind flow towards southern Africa and hence a decrease in rainfall (Fig. 3C, D, G and H). During SON, a strong presence and a southward shift of the semi-permanent anticyclones is still evident, although not as pronounced as during JJA (Fig. 2D and H). The corresponding increase in rainfall from JJA is evident in SON (Fig. 3D and H). The ERA-Interim dataset shows stronger values of high-pressure systems than the CMIP6 datasets.

In addition to the MSLP climatology, the 1018 isobar line was used to show the seasonality of the subtropical

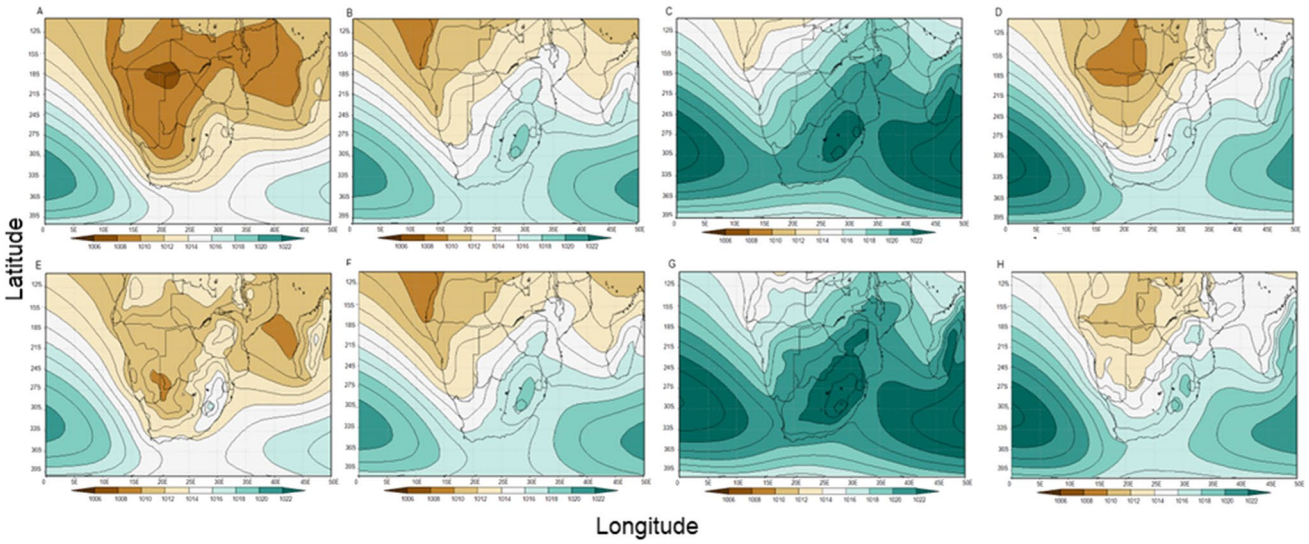


Fig. 2 Seasonal climatology of the sea level pressure (hPa) for **A** DJF, **B** MAM, **C** JJA and **D** SON for the CMIP6, and for **E** DJF, **F** MAM, **G** JJA and **H** SON for the ERA-Interim dataset. Green shades represent high-pressure values and brown shades represent low-pressure values

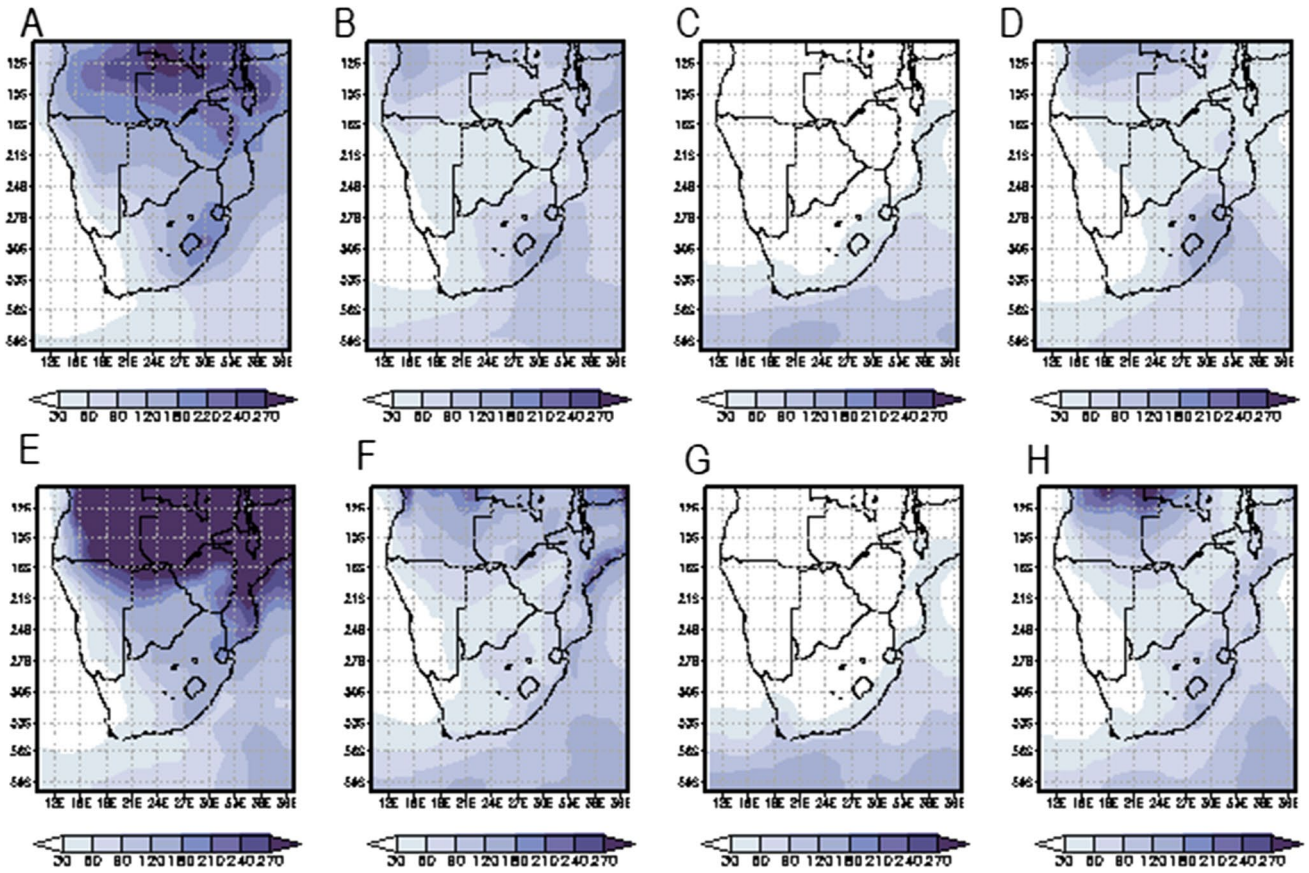


Fig. 3 Seasonal climatology of rainfall (mm) for **A** DJF, **B** MAM, **C** JJA and **D** SON for the CMIP6 and for **E** DJF, **F** MAM, **G** JJA and **H** SON for the ERA-Interim dataset. Light shades indicate lower rainfall totals and darker purple shades indicate higher rainfall totals

anticyclones (see Fig. 4). For all the seasons, the spatial extent of the 1018 hPa isobar is bigger for the ERA-Interim database and smaller for the CMIP6 ensemble mean. In JJA, the 1018 hPa isobar from the ERA-Interim database covers a larger area. It is located northwards from 12°S to 39°S. The 1018 hPa isobar for the CMIP6 data is a bit smaller and is located further south, i.e. from latitudes 15°S to 38°S. Although the difference is not that great, the spatial reduction of the 1018 hPa isobar is evident in SON. Its location is 16°S to 40°S and 22°S to 38°S for the ERA-Interim database and CMIP6 ensemble, respectively. During DJF and MAM, the 1018 hPa isobar covers a far smaller region than in JJA and SON. For the ERA-Interim database, the 1018 hPa isobar is located further south. Its position is 24°S to 38°S and 23°S to 38°S during DJF and MAM, respectively. For the CMIP6 ensemble, the 1018 hPa isobar is located at 27°S to 38°S and 27°S to 37°S during DJF and MAM, respectively.

The seasonality of the HC is clearly demonstrated in Fig. 5 for the CMPI6 ensemble mean and ERA-Interim (A−D) and ERA-Interim (E−H) average, respectively. Red and blue shades indicate an anticlockwise and a clockwise direction, respectively. During DJF and MAM, a less intense, narrow MMS exists, which is located more southwards (Fig. 5A, B, E and F). The anticlockwise circulation is more dominant in JJA and SON (Fig. 5C, D, G and H). Both the ERA-Interim and CMIP6 datasets show a more equatorward, stronger HC. Its southern flank is also more defined. However, there is a difference in the spatial representation of the maximum values of the MMS. The CMIP6 ensemble mean shows higher values of MMS for the clockwise circulation than the ERA-Interim datasets. One prominent feature in the representation of the MMS captured by both datasets is that the Southern Hemisphere subtropics are dominated by subsidence in all seasons.

3.1.3 Monthly climatology

The position and strength of the subtropical anticyclones during the various months of the year are further investigated by using the maximum values and latitudinal position of the SASA for the year (Fig. 6A and B). The ERA-Interim data displays higher values (Fig. 6A) with the SASA located more northward (Fig. 6B) than in the case of the CMIP6 ensemble mean for almost all months of the year. In both datasets, the austral summer and autumn months show the lowest values, with the SASA located the furthest south. February has the lowest SASA value. The southernmost position expressed by both datasets is for March. The highest values of the SASA are evident in July (ERA-Interim and CMIP6) and July (ERA-Interim). The northernmost position occurred in June, July and August.

3.2 Annual, seasonal and monthly trends

3.2.1 Annual trends

Annual trends of the MSLP, rainfall and MMS for both the CMIP6 ensemble average and the ERA-Interim database are shown in Fig. 7. Red contours indicate an increasing trend, and blue contours indicate a decreasing trend. Grey shades indicate areas of statistical significance. Increasing and statistically significant MSLP trends are evident from the ERA-Interim datasets for the entire country, as well as for the rest of the country. Statistical significance of the corresponding rainfall trends is evident throughout the country, demonstrated by an increase over the interior and a decrease east and west of the country (Fig. 7F). The negative values over areas of anticlockwise circulation represent the intensification of the subtropical dry zones (Held and Soden 2006).

3.2.2 Seasonal trends

Although the seasonal trends are not statistically significant, the CMIP6 data shows a tendency for the MSLP to increase over the interior and to the west of the country in DJF and JJA (Fig. 8A and C). Over the western parts of South Africa, an increasing trend is evident only for SON (Fig. 8D). A tendency for the MSLP to increase is still evident at seasonal scales from the ERA-Interim database

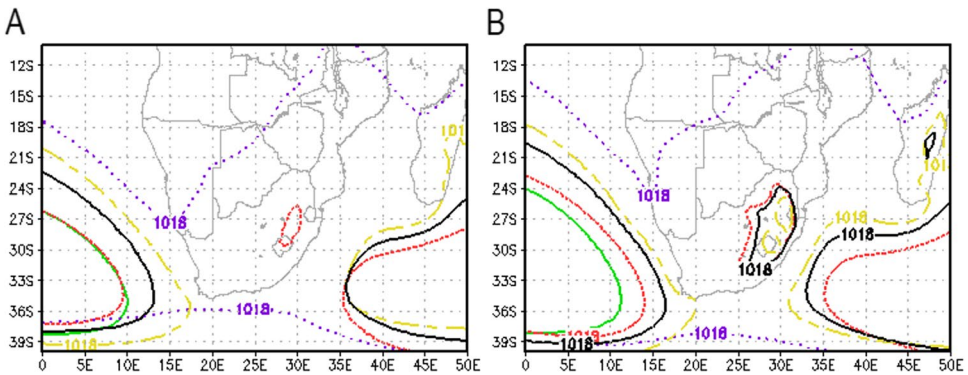


Fig. 4 Climatology of the 1018 hPa isobar for annual (solid black line), JJA (purple dotted line), SON (yellow big and small dashed line), MAM (red dotted line) and DJF (green solid line) for **A** the CMIP6 ensemble mean and **B** the ERA-Interim database

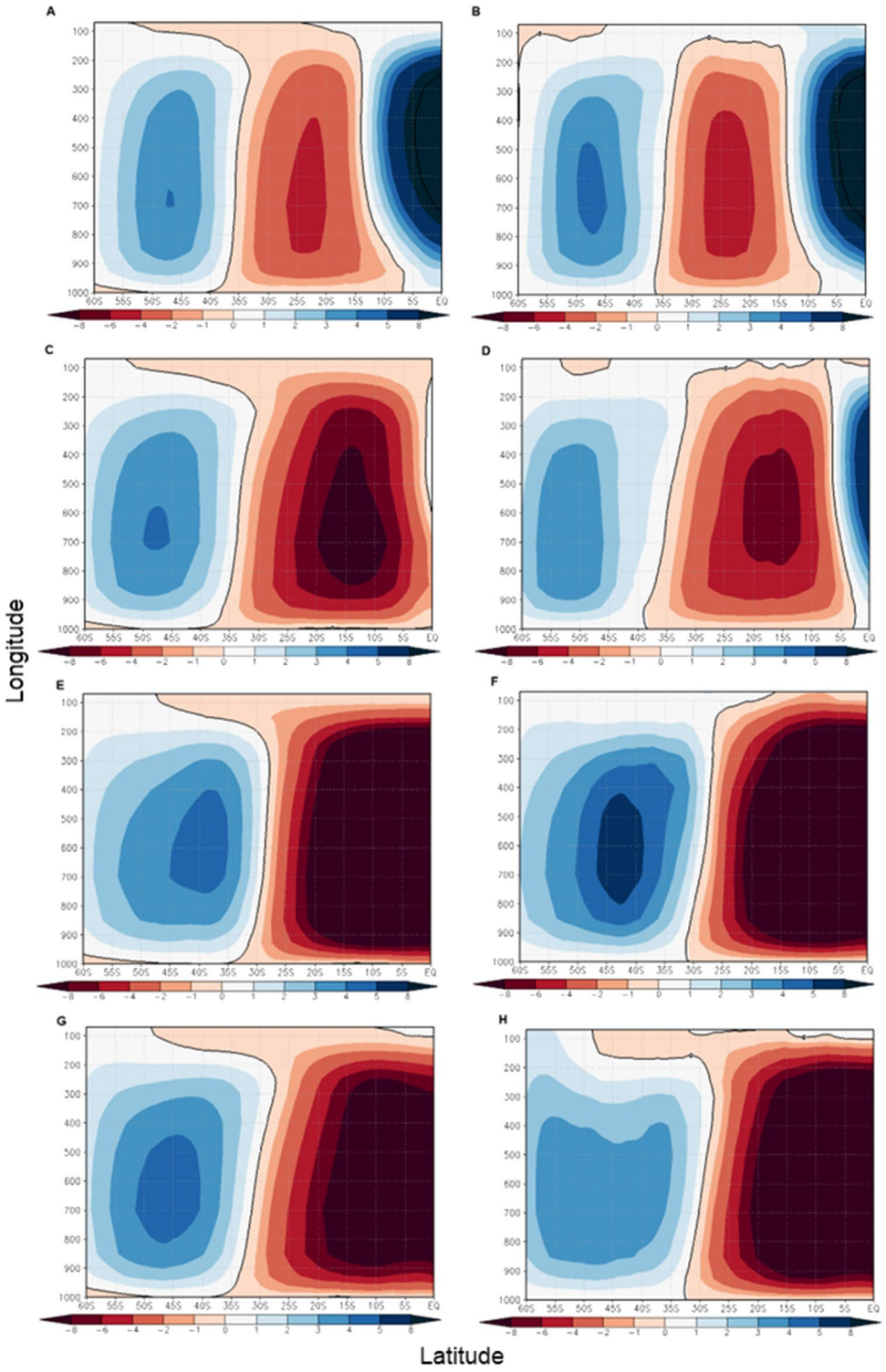


Fig. 5 Seasonal climatology of the meridional mass stream function ($\times 10^9$ kg s^{-1}) for **A** DJF, **B** MAM, **C** JJA and **D** SON for the CMIP6 ensemble mean and for **E** DJF, **F** MAM, **G** JJA and **H** SON for the ERA-Interim database. The red shades represent an anticlockwise circulation, and the blue shades represent a clockwise circulation

over the interior of the country (Fig. 8E–H). The highest increase is evident during the MAM season (Fig. 8F).

Trends in rainfall for the CMIP6 ensemble mean and the ERA-Interim database are illustrated in Fig. 9. The CMIP6 ensemble mean demonstrates relatively positive trends, although they are not statistically significant during DJF and MAM over most of the South African interior (Fig. 9A, B). A rainfall decrease is observed over the South African border of Mozambique and Zimbabwe during DJF, although this is over a smaller area. The CMIP6 MSLP

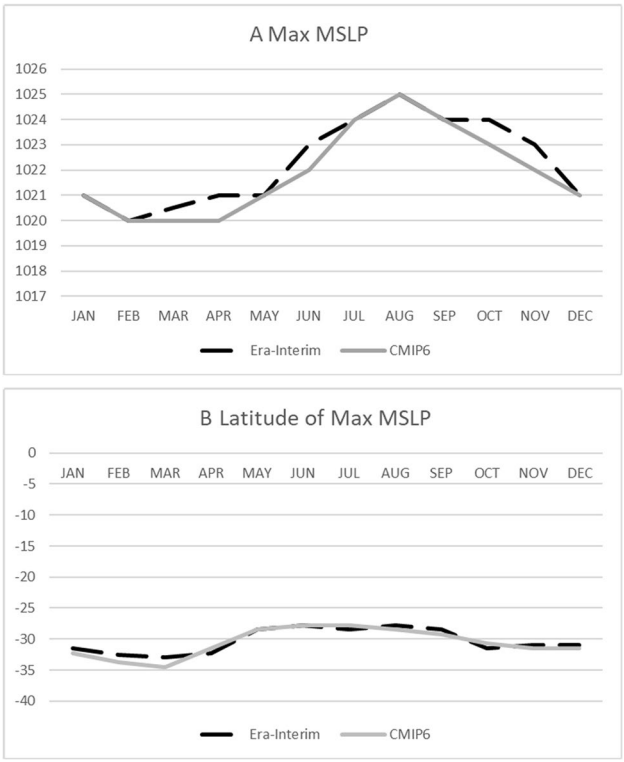


Fig. 6 The magnitude and latitude of the maximum sea level pressure for the CMIP6 ensemble mean (solid grey) and ERA-Interim database (black dash)

trends also show an increase over the interior of South Africa during DJF and JJA (Fig. 9A, C) and a decrease in MAM and SON (Fig. 9B, D). The statistical significance of the trends in the transition is more towards the north, south and east of South Africa.

The MMS trends for the ERA-Interim and CMIP6 data are shown in Fig. 10. Blue contours indicate the strengthening (weakening) of anticlockwise (clockwise) circulation, and red contours indicate the strengthening (weakening) of the clockwise (anticlockwise) circulation. Grey shades depict areas of statistical significance. The intensification is stronger for JJA, SON and DJF and weaker for MAM. The ERA-Interim data show a more northwards intensification than the CMIP6 ensemble mean. However, the intensification is more pronounced and less significant than for the CMIP6 ensemble mean (Fig. 10E, F). The trends analysis of the MMS shows a poleward migration for both datasets, indicating an expansion of the subtropical anticyclones.

3.2.3 Monthly trends

Monthly MMS trends for the CMIP6 ensemble mean and the ERA-Interim database are shown in Figs. 11 and 12, respectively. Blue contours indicate the strengthening (weakening) of anticlockwise (clockwise) circulation, and red contours indicate the strengthening (weakening) of the clockwise (anticlockwise) circulation. Grey shades depict areas of statistical significance. Rainfall trends from the CMIP6 ensemble mean show a tendency to decrease across the country for most of the months, and an increasing trend over the eastern parts of South Africa during the summer months. Increasing trends south of South Africa are evident in June and July for both datasets. For the ERA-Interim database, although also not significant, negative trends are evident in all months (Fig. 12A–L).

3.3 Model verification

A Taylor diagram summarising the performance of the CMIP6 GCMs in reproducing the Southern Hemisphere's mean mass stream function for DJF, MAM, JJA and SON is presented in Fig. 13A–D for each of the respective periods. The standard deviation of the reference data has been normalised to 1. The model's performance varies greatly from one season to the other. Although there is a strong spatial correlation between the GCMs and the ERA-Interim database, there is a wide spread of the GCMs and less correlation with the ERA-Interim database in DJF and MAM (Fig. 13A and B), and a narrow spread and greater correlation in JJA and SON (Fig. 13C and D). Normalised standard deviations (centred root mean square error (CRMSE)) range from 0.4 to 0.6 in DJF, 0.3 to 0.6 in MAM and 0.4 to 0.8 in SON. High values of standard deviation are evident in JJA. This means that most CMIP6 GCMs are able to capture the climatology of the MMS in the southern hemisphere in DJF and MAM and to a lesser extent in SON and JJA.

3.4 Climate Change Projections of the Hadley Cell, MSLP and South African Rainfall

Future projections of the seasonal MSLPs from the SSP126 and SSP585 are shown in Fig. 14. Green shades indicate an intensification of the subtropical high, while brown shades indicate the weakening. The 1018 hPa line is further used to show the position subtropical highs for the present-day climate, SSP126 and SSP585 scenarios. Intensification of the subtropical high is evident for all seasons for the different climate change scenarios. Both climate change projections indicate further southward's location of the 1018 hPa line than the history. The low mitigation scenario indicates more strengthening and further southward positioning of the subtropical high's than the high mitigation scenario.

Seasonal projections of the MMS (shaded plots) as well as the location of the HC Edge (solid lines) for the

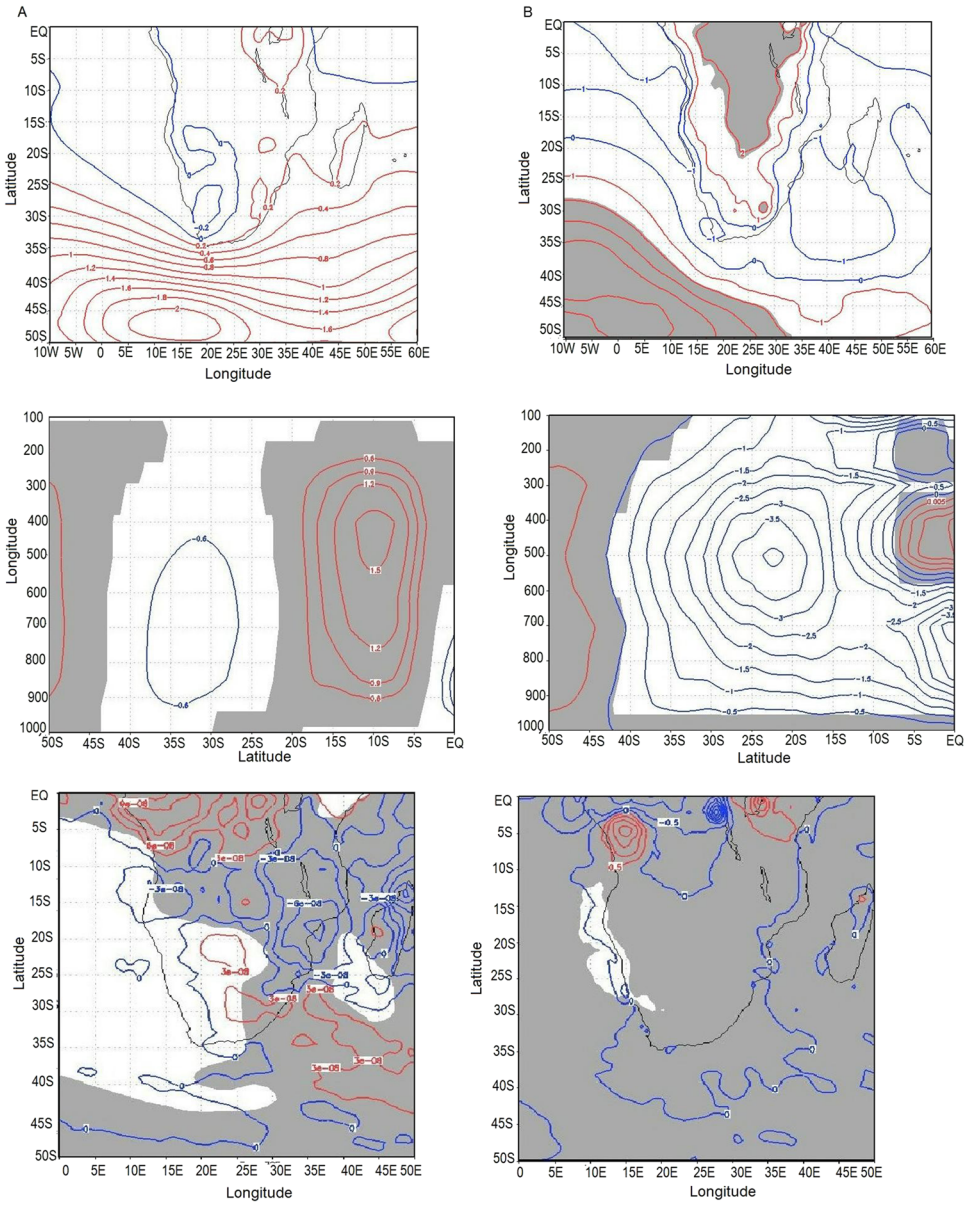


Fig. 7 Trends in annual MSLP (hPa), MMS (10^8 kg s^{-1}) and rainfall (mm) for the CMIP6 (**A**, **C** and **E**) and ERA-Interim (**B**, **D** and **F**) datasets, respectively. Blue contours represent a decreasing trend and red contours indicate an increasing trend. Grey shades indicate areas where the trends are statistically significant

present-day climate, SSP126 and SSP585 climate change scenarios from CMIP6 ensemble are shown in Fig. 15. Red shades indicate strengthening of the descending limb of the HC and blue shades indicate the weakening of the anticyclonic circulation. The intensification as well as the poleward shift of the HC is established from both the SSP126 and SSP585 climate change scenarios. The SSP585 displays a further southward shift than the SSP126 scenario. The shift in both MSLP and MMS projections under the low mitigation scenario indicate the poleward extension of the southern hemisphere subtropical dry zones (Mahlobo et al. 2018) and the intensification of the anticyclones (Fahad et al. 2021). The level of poleward expansion is less for the highly mitigated scenarios and more for the low mitigation scenarios. The projected southwards shift of the HC may be attributed to the increase in anthropogenic greenhouse gases and the stratospheric ozone hole over Antarctica (Hu et al. 2011; Scheff and Frierson 2012).

Figure 16 shows rainfall projections in different parts of South Africa. Rainfall increase is expected over the north-eastern parts of South Africa in summer for both scenarios (Fig. 16A and B), and this is attributed to the intensification of the continental trough counteracting the effects of the intensification of the HC. During the austral winter, rainfall is projected to decrease over the southwestern parts of South Africa under the low mitigation scenario (Fig. 16F) due to the increase in sea level pressure on the southern flank of the SASA and Mascarene High (Fig. 14F) as well

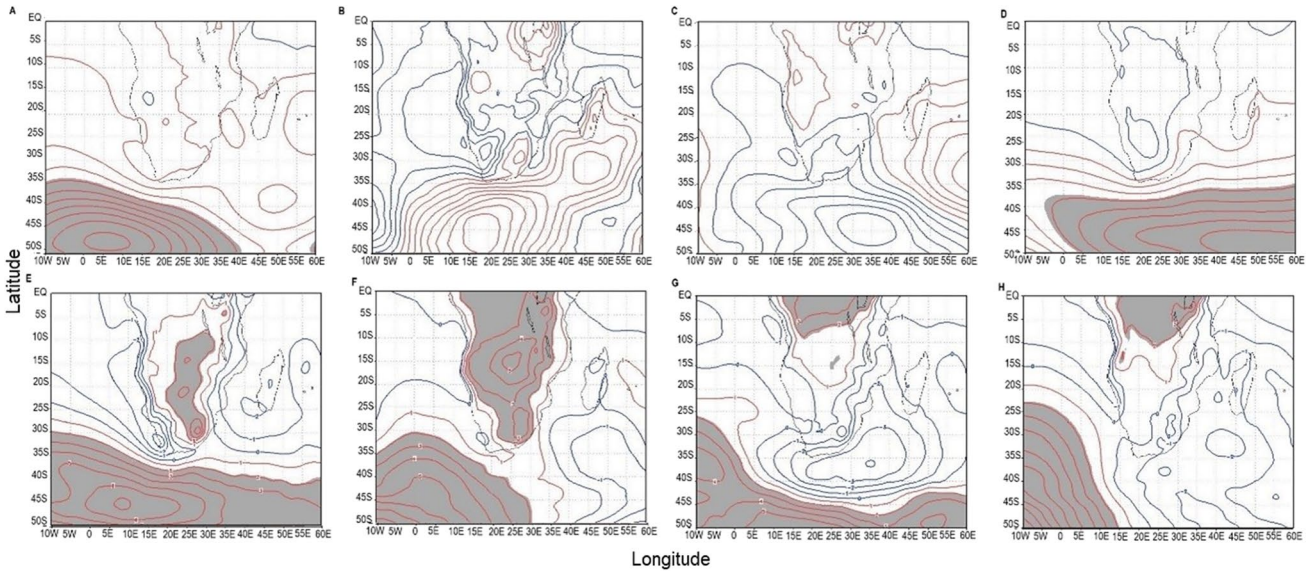


Fig. 8 Trends in the seasonal MSLP (hPa) for the CMIP6 ensemble mean for **A** DJF, **B** MAM, **C** JJA and **D** SON and for the ERA-Interim database for **E** DJF, **F** MAM, **G** JJA and **H** SON. Blue contours show a decreasing trend, and red contours indicate an increasing trend. Grey shades depict areas where the trends are statistically significant

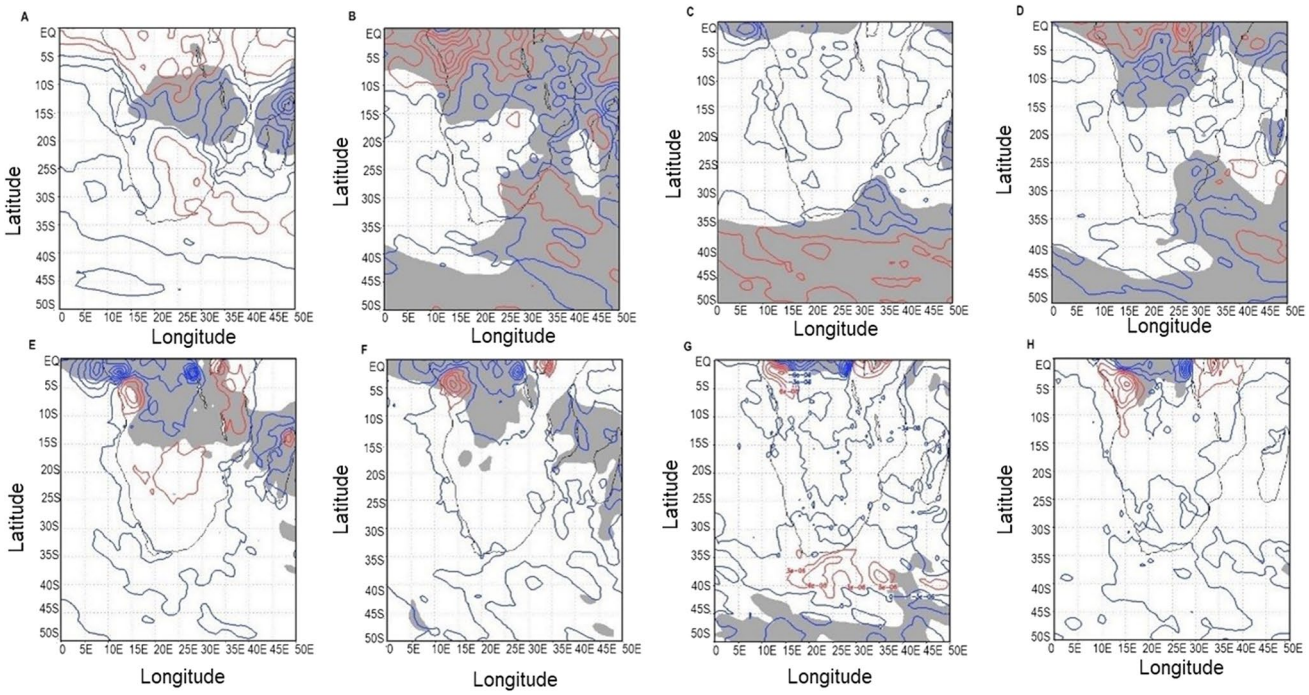


Fig. 9 Trends in seasonal rainfall (mm) for the CMIP6 ensemble mean for **A** DJF, **B** MAM, **C** JJA and **D** SON and for the ERA-Interim database for **E** DJF, **F** MAM, **G** JJA and **H** SON. Blue contours represent a decreasing trend and red contours indicate an increasing trend

the intensification and southward migration of the descending limb of the HC (Fig. 15E and F). Such changes will have different but devastating consequences for rainfall in the different regions of South Africa. For example, frontal rainfall will be limited to the east and north of the Karoo and Namib Deserts (Reason et al. 2002). The south-western parts of the country could experience an increase in the occurrence of day zero events due to the poleward shift

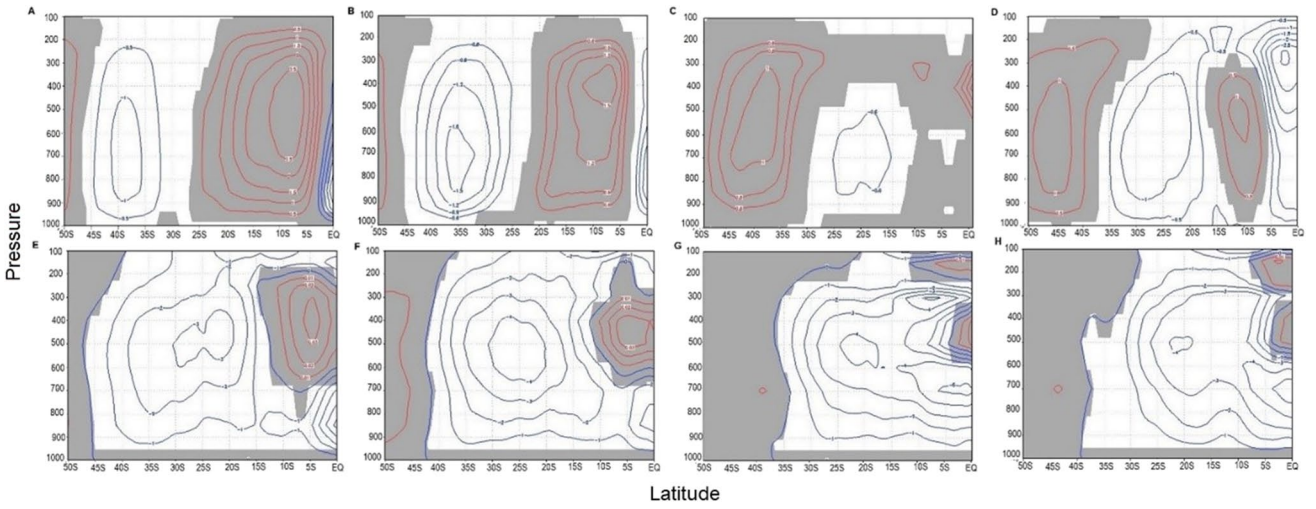


Fig. 10 Trends in the seasonal MMS (10^8 kg s^{-1}) for the CMIP6 ensemble mean for **A** DJF, **B** MAM, **C** JJA and **D** SON and for the Era-Interim database for **E** DJF, **F** MAM, **G** JJA and **H** SON. Blue contours indicate the strengthening (weakening) of anticlockwise (clockwise) circulation and red contours indicate the strengthening (weakening) of the clockwise (anticlockwise) circulation

of cold fronts, established from the MSLP southward. The interior of South Africa will experience more dry spells as well as a decrease in rainfall during autumn and spring (Engelbrecht and Landman 2010).

4 Summary

This study has presented evidence establishing connections between the subtropical high-pressure cells and the HC, which collectively influences South African rainfall patterns. These connections were explored through an analysis involving the ERA-Interim database and 14 GCMs from the CMIP6 project. Notably, the structure of the MMS is portrayed differently by the CMIP6 GCMs and the ERA-Interim database.

The 1018 hPa and maximum isobar in the study areas were used to analyse the subtropical anticyclones to determine the monthly MSLP. Both datasets portrayed the SASA west of the country, the Kalahari High over the interior of the country and the Mascarene High to the east of the country. However, the monthly, seasonal and annual CMIP6 ensemble averages indicate lower pressure values than the ERA-Interim dataset. The latitudinal position and strength of the MSLP also differ between the two datasets. The dominance of the Kalahari High during the summer months, and the north and south migration of the subtropical cyclones during the winter and summer months, respectively, were well captured and consistent with the HC's seasonal migration. This also corresponded with the climatology of seasonal rainfall over South Africa, characterised by rainfall over the eastern parts of South Africa during the austral summer, which also occurs more over the southwestern parts of the country during the winter months.

The study further used the Taylor diagram to investigate the performance of the individual GCMs in capturing the MMS in the southern hemisphere. The models showed a positive spatial correlation with the reanalysis. The weakest correlation and smaller standard deviation were observed during DJF and MAM, with a stronger correlation, but larger standard deviation in JJA and SON. This means that most CMIP6 GCMs are able to capture the climatology of the MMS in the southern hemisphere. A reasonable agreement was established between the models in JJA and SON, and less agreement in DJF and MAM.

According the CMIP6 MMS projections for SSP126 and SSP585 scenarios, the HC will continue to expand and shift southwards in the future. This is based on the increase in anthropogenic greenhouse gases and warming of the oceans, as well as the stratospheric ozone hole over Antarctica. Consequently, posited, the Southern Hemisphere anticyclones are projected to further intensify during summer and winter. Such changes will have different, but devastating consequences for rainfall in the different regions of South Africa. An increase in rainfall is expected over the northeastern parts of South Africa in summer. This is attributed to the intensification of the continental trough, counteracting the effects of the intensification of the HC. During the austral winter, rainfall is projected to decrease over the southwestern parts of South Africa. This is attributed to an increase in sea level pressure on the southern flank of the SASA and the Mascarene high.

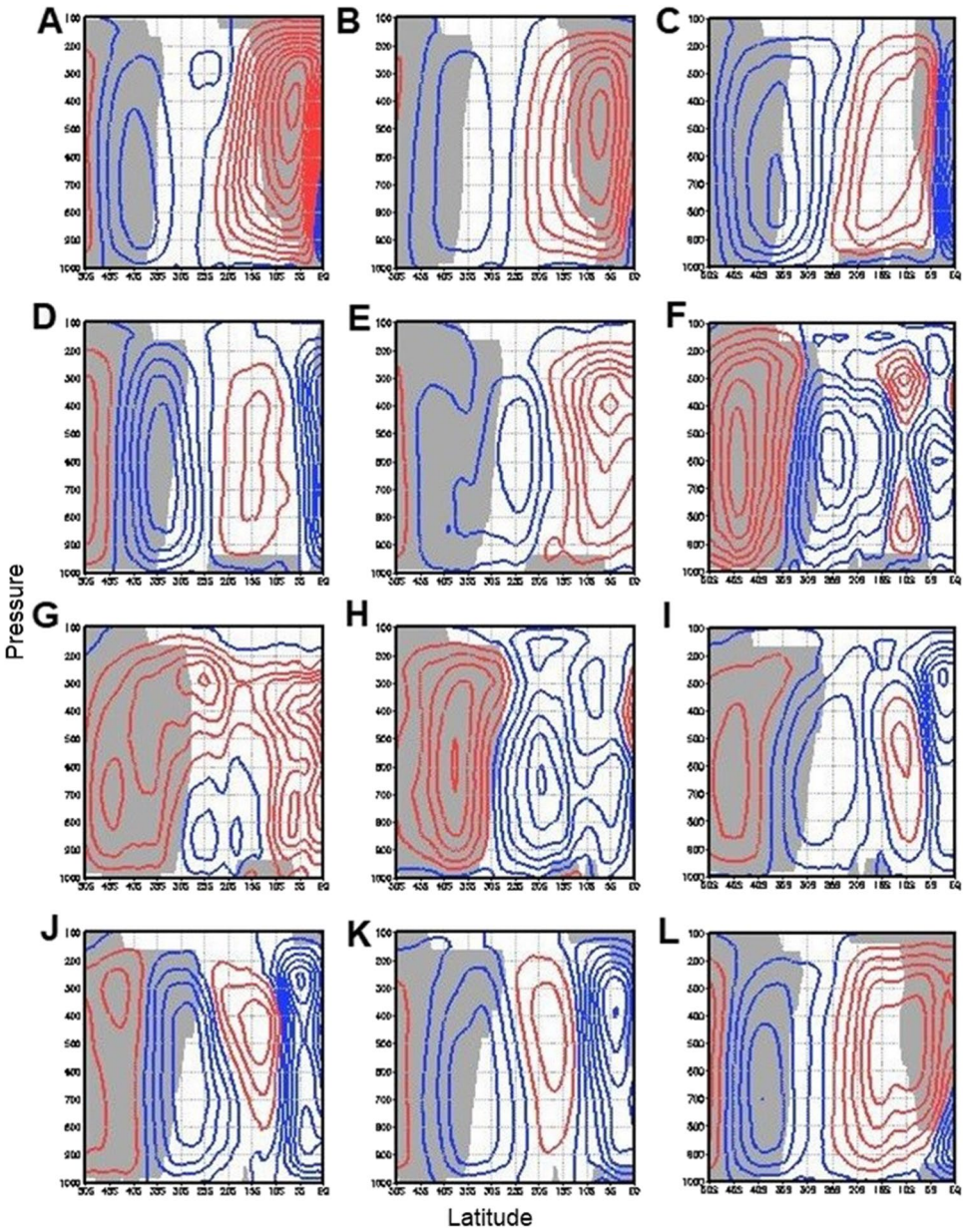


Fig. 11 Monthly MMS (10^8 kg s^{-1}) trends in **A** January, B February, **C** March, **D** April, **E** May, **F** June, **G** July, **H** August, **I** September, **J** October, **K** November and **L** December for the CMIP6 ensemble mean. Blue contours indicate the strengthening (weakening) of anticlockwise (clockwise) circulation, and red contours indicate the strengthening (weakening) of the clockwise (anticlockwise) circulation. Grey shades depict areas where the trends are statistically significant

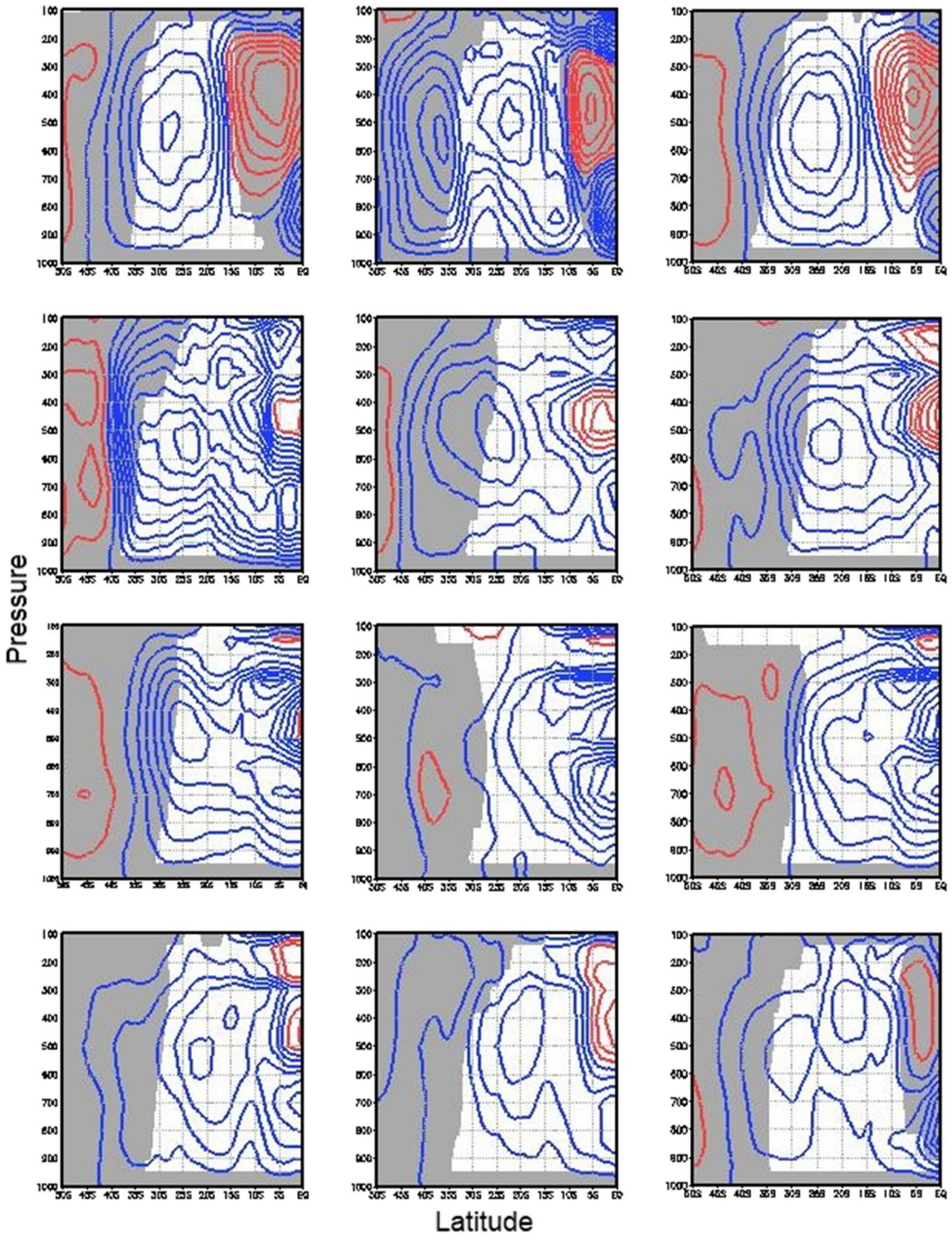


Fig. 12 Monthly MMS trends (10^8 kg s^{-1}) in **A** January, **B** February, **C** March, **D** April, **E** May, **F** June, **G** July, **G** August, **I** September, **J** October, **K** November and **L** December for the ERA-Interim database. Blue contours indicate the strengthening (weakening) of anticlockwise (clockwise) circulation, and red contours indicate the strengthening (weakening) of the clockwise (anticlockwise) circulation. Grey shades depict areas where the trends are statistically significant

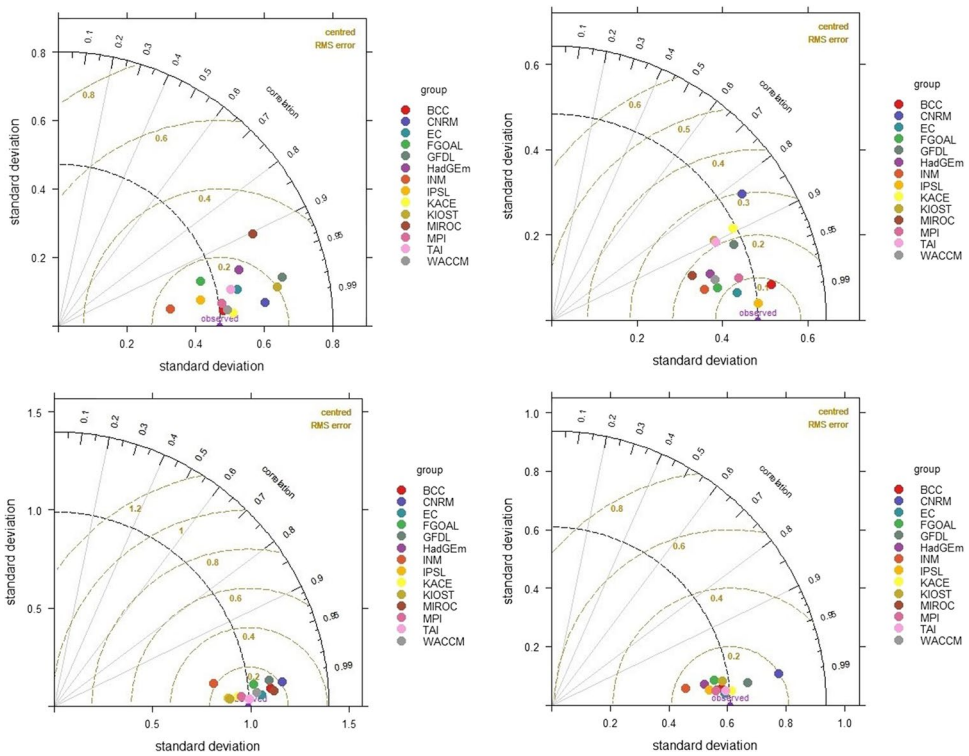


Fig. 13 The Taylor diagrams showing the performance of 14 CMIP6 GCMs in simulating the 39-year climatology of the MMS in the Southern Hemisphere for **A** DJF, **B** MAM, **C** JJA and **D** SON

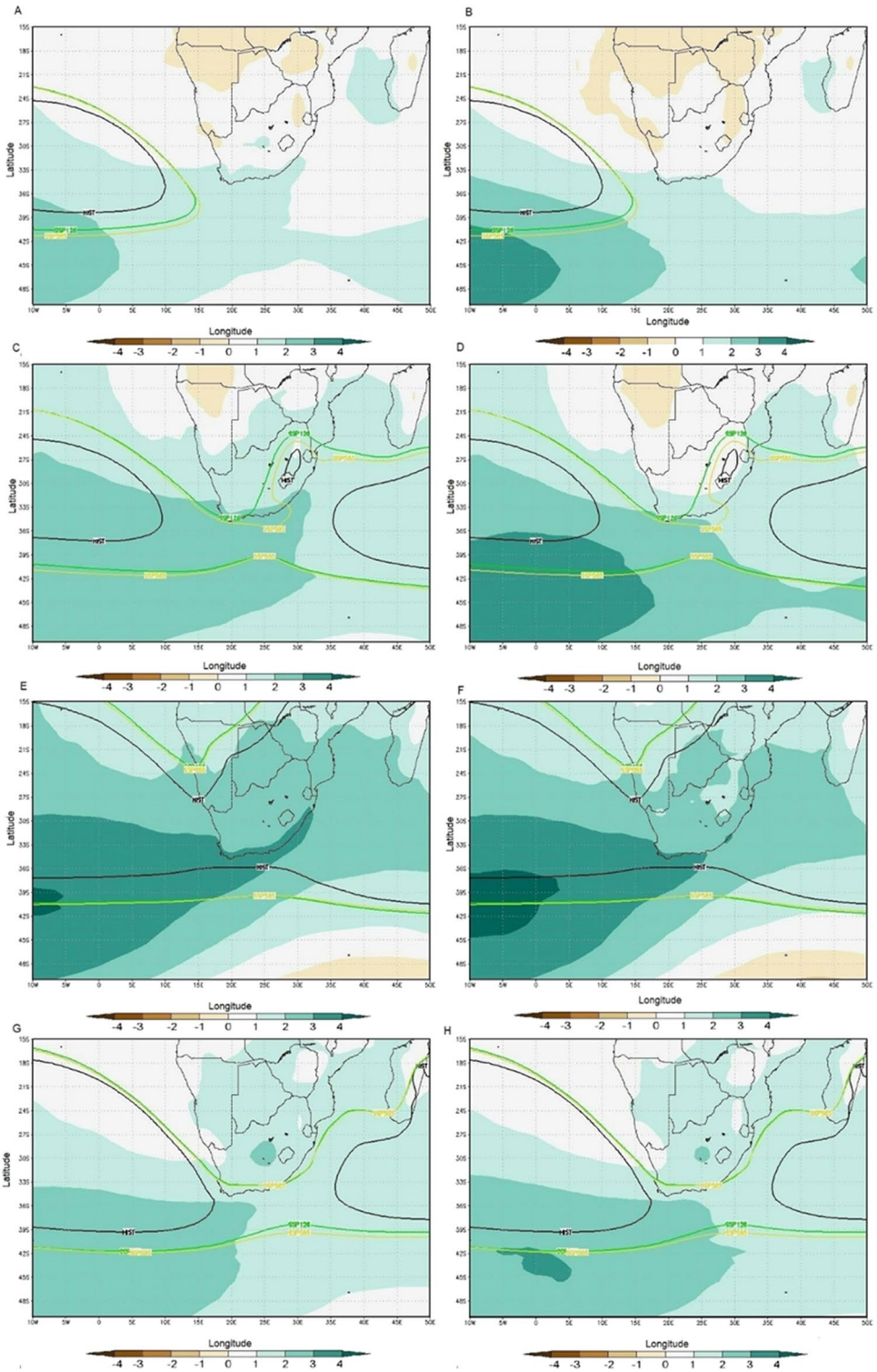


Fig. 14 Projected change in seasonal MSLP (hPa) for SSP12: **A** SSP126 DJF, **B** SSP585 DJF, **C** SSP126 MAM, **D** SSP58 MAM, **E** SSP126 JJA, **F** SSP585 JJA, **G** SSP126 SON and **H** SSP 585 SON CMIP6 ensemble mean. Green shades represent increase in MSLP, and brown shades represents increase in MSLP. Solid lines indicate the position of the 1018hPa line for the present-day climate, SSP126 and SSP585 scenarios

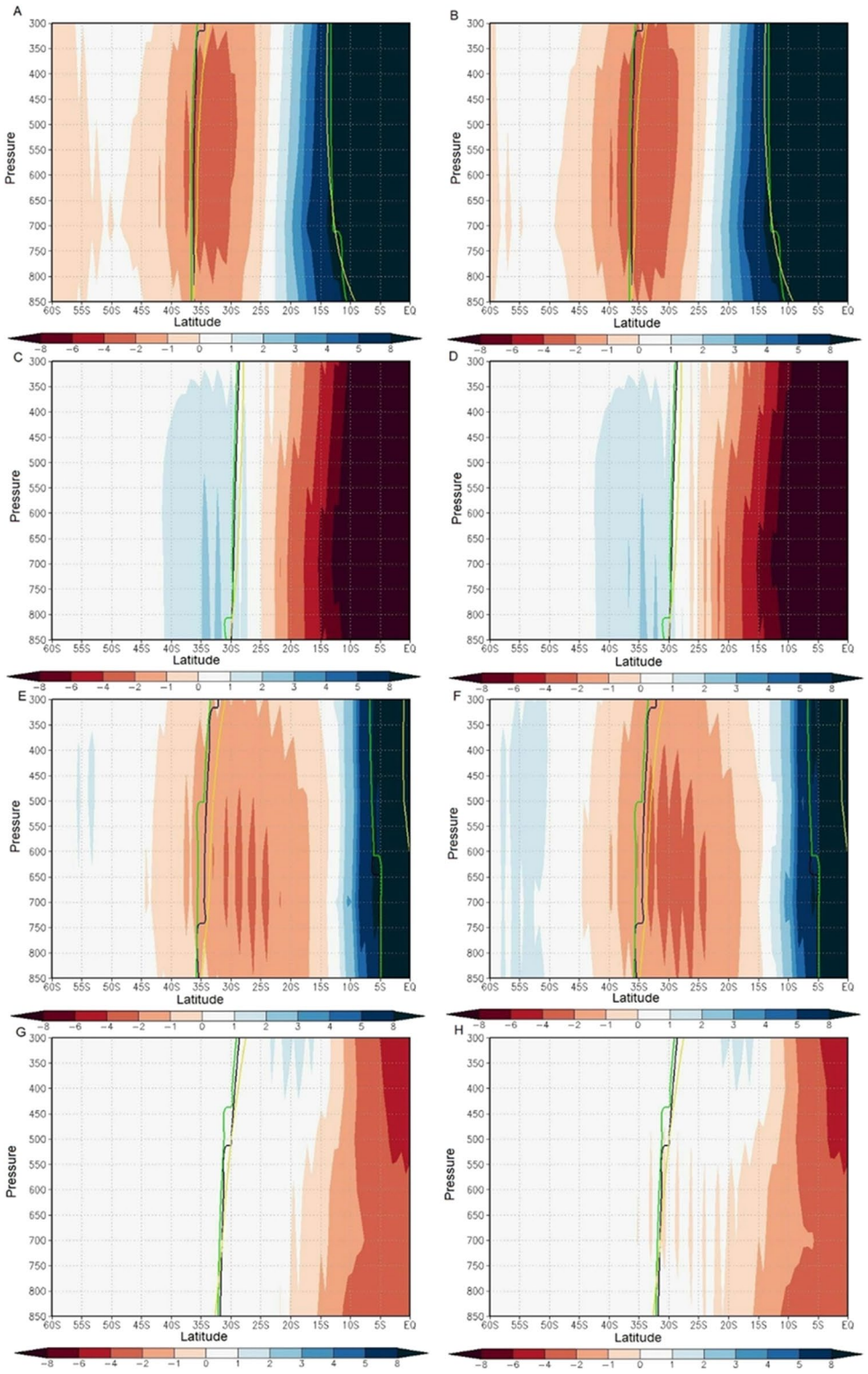


Fig. 15 Projected change in seasonal meridional mass stream function ($\times 10^9$ kg s^{-1}) for SSP12: **A** SSP126 DJF, **B** SSP585 DJF, **C** SSP126 MAM, **D** SSP58 MAM, **E** SSP126 JJA, **F** SSP585 JJA, **G** SSP126 SON and **H** SSP 585 SON CMIP6 ensemble mean. Red shades represent decrease in MMS and blue shades represents increase in MMS. Solid lines indicate a zero MMS for the present-day (yellow) SSP126 (black), SSP585 (green)

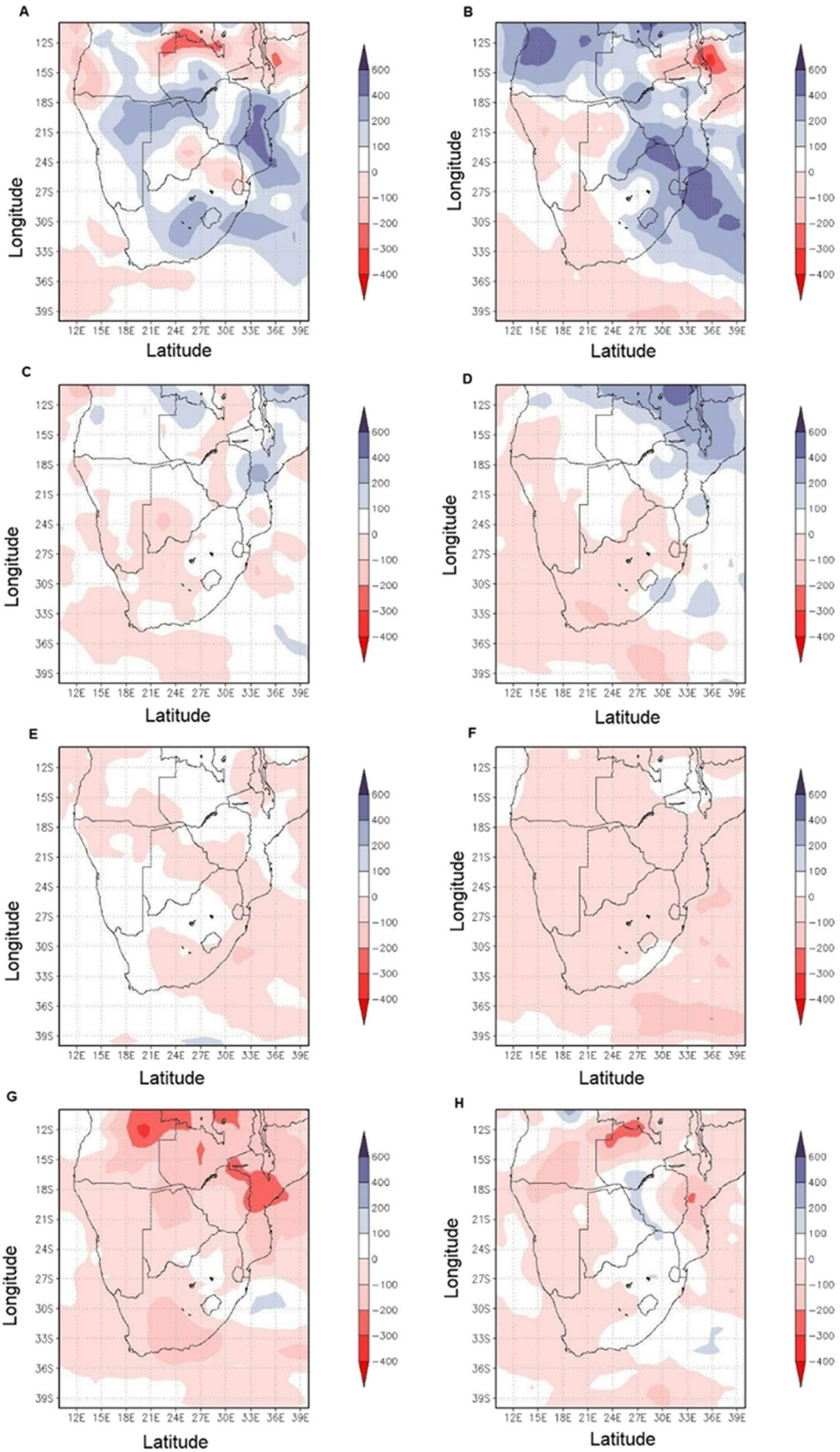


Fig. 16 Projected change in seasonal rainfall (mm) for SSP12: **A** SSP126 DJF, **B** SSP585 DJF, **C** SSP126 MAM, **D** SSP58 MAM, **E** SSP126 JJA, **F** SSP585 JJA, **G** SSP126 SON and **H** SSP585 SON CMIP6 ensemble mean. Red shades represent rainfall reduction and blue shades represents rainfall increase

Code availability Not applicable

Author contributions The first draft of the manuscript was written by D Mahlobo. F Engelbrecht, T Ndarana and MF Olabanji commented on previous versions of the manuscript. All authors read and approved the final manuscript.

Data availability The datasets generated during and/or analysed during the current study are available from the corresponding author on reasonable request.

Declarations

Ethics approval/declarations (include appropriate approvals or waivers) Not applicable

Consent to participate Not applicable

Consent for publication (include appropriate statements) Not applicable

Competing interests The authors declare no competing interests.

Open Access This article is licensed under a Creative Commons Attribution 4.0 International License, which permits use, sharing, adaptation, distribution and reproduction in any medium or format, as long as you give appropriate credit to the original author(s) and the source, provide a link to the Creative Commons licence, and indicate if changes were made. The images or other third party material in this article are included in the article's Creative Commons licence, unless indicated otherwise in a credit line to the material. If material is not included in the article's Creative Commons licence and your intended use is not permitted by statutory regulation or exceeds the permitted use, you will need to obtain permission directly from the copyright holder. To view a copy of this licence, visit http://creativecommons.org/licenses/by/4.0/.

References

Allen RJ, Sherwood SC, Norris JR, Zender C (2012) Recent Northern Hemisphere tropical expansion primarily driven by black carbon and tropospheric ozone. Nature 485:350–355

Boer GJ, Smith DM, Cassou C, Doblas-Reyes F, Danabasoglu G, Kirtman B, Kushnir Y, Kimoto M, Meehl GA, Msadek R, Mueller WA (2016) The decadal climate prediction project (DCPP) contribution to CMIP6. Geosci Model Dev 9(10):3751–3777

Burls NJ, Blamey RC, Cash BA, Swenson ET, Fahad AA, Bopape MJ, Straus DM, Reason CJC (2019) The Cape Town "Day Zero" drought and HC expansion. NPJ Clim Atmos Sci 2(1):1–8

Chen G, Held IM (2007) Phase speed spectra and the recent poleward shift of Southern Hemisphere surface westerlies. Geophys Res Lett 34:L21805. https://doi.org/10.1029/2007GL031200

Cherchi A, Ambrizzi T, Behera S, Freitas ACV, Morioka Y, Zhou T (2018) The response of subtropical highs to climate change. Curr Clim Change Rep 4(4):371–382

Cook KH (2003) Role of continents in driving the Hadley cells. J Atmos Sci 60:957–976

Dee DP, Uppala SM, Simmons AJ, Berrisford P, Poli P, Kobayashi S, Andrae U, Balmaseda MA, Balsamo G, Bauer DP, Bechtold P (2011) The ERA-Interim reanalysis: configuration and performance of the data assimilation system. Q J R Meteorol Soc 137(656):553–597

Diaz HF, Bradley RS (2004) The Hadley circulation: present, past, and future: an introduction. In: The Hadley circulation: present, past and future. Springer, Netherlands: Dordrecht, pp 1–5

Dima IM, Wallace JM (2003) On the seasonality of the HC. J Atmos Sci 60(12):1522–1527

Engelbrecht F, Landman W (2010) A brief description of South Africa's present-day climate. South African Risk and Vulnerability Atlas. Department of Science and Technology, Republic of South Africa, Pretoria, p 62

Engelbrecht FA, Landman WA, Engelbrecht CJ, Landman S, Bopape MM, Roux B, McGregor JL, Thatcher M (2011) Multi-scale climate modelling over southern Africa using a variable-resolution global model. Water SA 37:647–658

Engelbrecht FA, McGregor JL, Engelbrecht CJ (2009) Dynamics of the conformal-cubic atmospheric model projected climate-change signal over southern Africa. Int J Climatol 29:1013–1033

Fahad AA, Burls N, Swenson E, Straus D (2021) The influence of South Pacific convergence zone heating on the South Pacific subtropical anticyclone. J Clim 34(10):3787–3798

Freitas ACV, Ambrizzi T (2015) Recent changes in the annual mean regional HC and their impacts on South America. Adv Meteorol 22

Frierson DMW, Lu J, Chen G (2007) Width of the HC in simple and comprehensive general circulation models. Geophys Res Lett 34. https://doi.org/10.1029/2007GL031115

Fu Q, Johanson CM, Wallace JM, Reichler T (2006) Enhanced midlatitude tropospheric warming in satellite measurements. Science 312(5777):1179–1179

Held IM, Soden BJ (2006) Robust responses of the hydrological cycle to global warming. J Clim 19(21):5686–5699

Holton JR, Hakim GJ (2012) An introduction to dynamic meteorology. Academic Press, Burlington

Hoskins B (1996) On the existence and strength of the summer subtropical anticyclones. Bull Am Meteorol Soc 77:1287–1292

Hou AY, Lindzen RS (1992) The influence of concentrated heating on the Hadley Circulation. J Atmos Sci 49:1233–1241

Hu Y, Zhou C, Liu J (2011) Observational evidence for poleward expansion of the Hadley circulation. Adv Atmos Sci 28:33–44

Hu Y, Tao L, Liu J (2013) Poleward expansion of the Hadley circulation in CMIP5 simulations. Adv Atmos Sci 30:790–795

Jakobson E, Vihma T, Palo T, Jakobson L, Keernik H, Jaagus J (2012) Validation of atmospheric reanalyses over the central Arctic Ocean. Geophys Res Lett 39(10)

Johanson CM, Fu Q (2009) Hadley cell widening: model simulations versus observations. J Clim 22:2713–2725

Kanamitsu M, Krishnamurti TN (1978) Northern summer tropical circulations during drought and normal rainfall months. Mon Weather Rev 106:331–347

Lee SK, Mechoso CR, Wang C, Neelin JD (2013) Interhemispheric influence of the northern summer monsoons on southern subtropical anticyclones. J Clim 26(24):10193–10204

Li L, Li W, Kushnir Y (2012) Variation of the North Atlantic subtropical high western ridge and its implication to Southeastern US summer precipitation. Clim Dyn 39(6):1401–1412

Lin R, Zhou T, Qian Y (2014) Evaluation of global monsoon precipitation changes based on five reanalysis datasets. J Clim 27(3):1271–1289

Liu J, Song M, Hu Y, Ren X (2012) Changes in the strength and width of the Hadley circulation since 1871. Clim Past 8(4):1169–1175

Lu J, Vecchi GA, Reichler T (2007) Expansion of the HC under global warming. Geophys Res Lett 34:L06805. https://doi.org/10.1029/2006GL028443

Mahlalela PT, Blamey RC, Reason CJC (2019) Mechanisms behind early winter rainfall variability in the southwestern Cape. South Africa Clim Dyn 53(1):21–39

Mahlobo DD, Ndarana T, Grab S, Engelbrecht F (2018) Integrated climatology and trends in the subtropical HC, sunshine duration and cloud cover over South Africa. Int J Climatol 39(4):1805–1821

Manabe S, Holloway JL (1975) The seasonal variation of the hydrological cycle as simulated by a global model of the atmosphere. J Geophys Res-Atmos 80:1617–1649

Mitas CM, Clement A (2005) Has the Hadley cell been strengthening in recent decades? Geophys Res Lett 32(3)

Namias J (1972) Influence of northern hemisphere general circulation on drought in northeast Brazil 1. Tellus 24:336–343

Nguyen H, Evans A, Lucas C, Smith I, Timbal B (2013) The Hadley circulation in reanalyses: climatology, variability and change. J Clim 26:3357–3376

Nguyen H, Lucas C, Evans A, Timbal B, Hanson L (2015) Expansion of the Southern Hemisphere Hadley cell in response to greenhouse gas forcing. J Clim 28(20):8067–8077

Nicholson SE (1981) Rainfall and atmospheric circulation during drought periods and wetter years in West Africa. Mon Weather Rev 109(10):2191–2208

Pascale S, Kapnick SB, Delworth TL, Cooke WF (2020) Increasing risk of another Cape Town "Day Zero" drought in the 21st century. Proc Natl Acad Sci 117(47):29495–29503

Polvani LM, Waugh DW, Correa GJ, Son SW (2011) Stratospheric ozone depletion: the main driver of twentieth-century atmospheric circulation changes in the Southern Hemisphere. J Clim 24(3):795–812

Rapolaki RS, Blamey RC, Hermes JC, Reason CJC (2020) Moisture sources associated with heavy rainfall over the Limpopo River Basin, southern Africa. Clim Dyn 55:1473–1487

Reason CJC, Rouault M, Melice JL, Jagadheesha D (2002) Interannual winter rainfall variability in SW South Africa and large-scale ocean-atmosphere interactions. Meteorog Atmos Phys 80(1):19–29

Reboita MS, Ambrizzi T, Silva BA, Pinheiro RF, Da Rocha RP (2019) The South Atlantic subtropical anticyclone: present and future climate. Front Earth Sci 7:8

Rodwell MJ, Hoskins BJ (2001) Subtropical anticyclones and summer monsoons. J Clim 14(15):3192–3211

Roffe SJ, Fitchett JM, Curtis CJ (2019) Classifying and mapping rainfall seasonality in South Africa: a review. S Afr Geogr J/Suid-Afrikaanse Geografiese Tydskrif 101(2):158–174

Scheff J, Frierson DM (2012) Robust future precipitation declines in CMIP5 largely reflect the poleward expansion of model subtropical dry zones. Geophys Res Lett 39(18)

Schwendike J, Berry GJ, Reeder MJ, Jakob C, Govekar P, Wardle R (2015) Trends in the local Hadley and local Walker circulations. J Geophys Res Atmos 120(15):7599–7618

Schwendike J, Govekar P, Reeder MJ, Wardle R, Berry GJ, Jakob C (2014) Local partitioning of the overturning circulation in the tropics and the connection to the Hadley and Walker circulations. J Geophys Res Atmos 119(3):1322–1339

Seager R, Murtugudde R, Naik N, Clement A, Gordon N, Miller J (2003) Air-sea interaction and the seasonal cycle of the subtropical anticyclones. J Clim 16(12):1948–1966

Seidel DJ, Randel WJ (2007) Recent widening of the tropical belt: evidence from tropopause observations. J Geophys Res 112:D020113

Solomon S, Qin D, Manning M, Chen Z, Marquis M, Averyt KB, Tignor M, Miller HL (2007) Summary for policymakers. In: Climate Change 2007: Synthesis Report. In: Contribution of Working Group I, II and III to the Fourth Assessment Report of the Intergovernmental Panel on Climate Change. Cambridge University Press, Cambridge and New York

Sousa PM, Blamey RC, Reason CJ, Ramos AM, Trigo RM (2018) The 'Day Zero' Cape Town drought and the poleward migration of moisture corridors. Environ Res Lett 13(12):124025

Taljaard JJ (1996) Atmospheric circulation systems, synoptic climatology and weather phenomena of South Africa. Part 6: Rainfall in South Africa. South African Weather Bureau, Technical paper 32

Trenberth KE, Fasullo JT, Kiehl J (2009) Earth's global energy budget. Bull Am Meteorol Soc 90(3):311–324

Tyson PD, Preston-Whyte RA (2000) The weather and climate of Southern Africa. Oxford University Press, p 396

Vigaud N, Richard Y, Rouault M, Fauchereau N (2009) Moisture transport between the South Atlantic Ocean and southern Africa: relationships with summer rainfall and associated dynamics. Clim Dyn 32(1):113–123

Xulu NG, Chikoore H, Bopape MM, Nethengwe NS (2020) Climatology of the Mascarene high and its influence on weather and climate over Southern Africa. Climate 8:86. https://doi.org/10.3390/cli8070086

Yin JH (2005) A consistent poleward shift of the storm tracks in simulations of 21st century climate. Geophys Res Lett 32:L18701

Ynoue RY, Reboita MS, Ambrizzi T, Da Silva GA (2017) Meteorology: the basics. Ed. Oficina de Textos, São Paulo

Publisher's note Springer Nature remains neutral with regard to jurisdictional claims in published maps and institutional affiliations.